BEAM-PROFILE INSTRUMENTATION FOR A BEAM-HALO MEASUREMENT: OVERALL DESCRIPTION, OPERATION, AND BEAM DATA•

J. D. Gilpatrick, D. Barr, L. Day, D. Kerstiens, M. Stettler, R. Valdiviez, Los Alamos National Laboratory
M. Gruchalla, J. O'Hara, Honeywell Corporation
J. Kamperschroer, General Atomics Corporation

Abstract

The halo experiment presently being conducted at the Low Energy Demonstration Accelerator (LEDA) at Los Alamos National Laboratory (LANL) has specific instruments that acquire horizontally and vertically projected particle-density beam distributions out to greater than 105:1 dynamic range. We measure the core of the distributions using traditional wire scanners, and the tails of the distribution using water-cooled graphite scraping devices. The wire scanner and halo scrapers are mounted on the same moving frame whose location is controlled with stepper motors. A sequence within the Experimental Physics and Industrial Control System (EPICS) software communicates with a National Instrument LabVIEW virtual instrument to control the movement and location of the scanner/scraper assembly. Secondary electrons from the wire scanner 33-μm carbon wire and protons impinging on the scraper are both detected with a lossy-integrator electronic circuit. Algorithms implemented within EPICS and in Research Systems' Interactive Data Language (IDL) subroutines analyse and plot the acquired distributions. This paper describes the beam profile instrument, describes our experience with its operation, compares acquired profile data with simulations, and discusses various beam profile phenomenon specific to the halo experiment.

1 HALO INSTRUMENTATION

At LEDA a 100-mA, 6.7-MeV beam is injected into a 52-quadrupole magnet lattice (see fig. 1). Within this 11-m FODO lattice, there are nine wire scanner/halo scraper/wire scanner (WS/HS) stations, five pairs of steering magnets and beam position monitors, five loss monitors, three pulsed-beam current monitors, and two image-current monitors for monitoring beam energy (2). The WS/HS instrument's purpose is to measure the beam's transverse projected distribution. These measured distributions must have sufficient detail to understand beam halo resulting from upstream lattice mismatches. The first WS/HS station, located after the fourth quadrupole magnet, verifies the beam's transverse characteristics after the RFQ exit. A cluster of four HS/WS located after magnets #20, #22, #24, and #26 provides phase space information after the beam has debunched. After magnets #45, #47, #49, and #51 reside the final four WS/HS stations. These four WS/HS acquire projected beam distributions under both matched and mismatched conditions. These conditions are generated by adjusting the first four quadrupole magnets fields so that the RFQ output beam is matched or mismatched in a known fashion to the rest of the lattice. Because the halo takes many lattice periods to fully develop, this final cluster of WS/HS are positioned to be most sensitive to halo generation.

Figure 1. The 11-m, 52-magnet FODO lattice includes nine WS/HS stations that measure the beam's transverse projected distributions.

As the RFQ output beam is mismatched to the lattice, the WS/HS actually observe a variety of distortions to a properly matched gaussian-like distribution (1,3). These distortions appear as distribution tails or backgrounds. It is the size, shape, and extent of these tails that predicts specific type of halo. However, not every lattice WS/HS observes the halo generated in phase space because the resultant distribution tails may be hidden from the projection's view. Therefore, multiple WS/HS are used to observe the various distribution tails.

2 WS/HS DESCRIPTION

Each station consists of a horizontal and vertical actuator assembly (see fig. 2) that can move a 33-μm-carbon monofilament and two graphite/copper scraper sub-

assemblies (4). The carbon wire and scrapers are connected to the same movable frame. Attached to this movable frame is a linear encoder that provides the wire and scraper edges' relative position to within 5 μm, an additional linear potentiometer provides an absolute approximate position for LEDA's run permit systems. A stepper motor and ball lead screw drive the actuated moveable frame, and microswitches and motor brakes limit the wire and scraper movement.

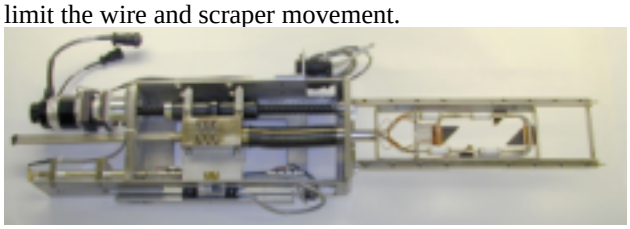

Figure 2. The WS/HS assembly contains a movable frame on which a 0.03-mm carbon wire resides between two water-cooled graphite scrapers.

The carbon wire, which senses the beam's core, is cooled by thermal radiation. If the beam macropulse is too long, the wire temperature continues above 1800 K resulting in the onset of thermionic emission. Thermionic emission gives the distribution an inaccurate appearance of a larger distribution core current density. To eliminate these effects for the halo experiment, the maximum pulse length and repetition rate is limited to approximately 30 ms and 1 Hz, respectively.

The halo scrapers are composed of a 1.5-mm thick graphite plate brazed to a water-cooled 1.5-mm thick copper plate. Since 6.7-MeV protons average range in carbon is approximate 0.3 mm, the beam is completely stopped within the graphite plate. Cooling via conduction lowers the average temperature of scraper sub-assembly and allows the scraper to be cooled more rapidly than the wire. The lower average temperature and faster cooling allows the scraper to be driven in as far as 2 rms widths from the beam distribution peak without the peak temperature increasing above 1800 K.

The movement and positioning of each wire and scraper pair is controlled by a movement control system that contains a stepper motor, stepper motor controller, a linear encoder, and an electronic driver amplifier. The controller's digital PID loop controls the speed and accuracy at which the assembly is moved and placed.

The target position, as defined by the WS/HS operator, is relayed from the EPICS control screen via a database process variable to a National Instruments LabVIEW Virtual Instrument (VI). The VI also calibrates the relative position of the linear encoders based on the measured position of the limit switches, and provides some error feedback information. The total error between the target wire position and the actual position attained are <+/-2% of a 1-mm width beam (see fig. 3).

beam's energy is imparted to the wire causing secondary electron emission to occur. The secondary electrons leaving the wire are replaced by negative charge flowing from the electronics. This current flow for both axes is connected through a bias battery to an electronic lossy integrator circuit and followed by an amplification stage.

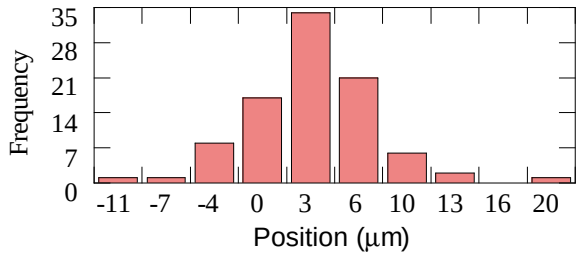

Figure 3. The above histogram shows a typical distribution of wire/scraper movement errors.

The integrator capacitance and amplifier gain are set to allow a very wide range of values of accumulated charge. Data are acquired by digitising the accumulated charge through the lossy integrator at two different times within the beam pulse. This charge difference acquired by subtracting the two values of charge provides a low noise method of relative beam charge acquisition. The wire and scraper accumulated charge signals are digitised using 12-bit digitisers. The analogue noise floor has been measured to be 0.03 pC, a noise level slightly lower than the scraper digital LSB noise level of 0.6 pC using the highest gain settings within the detection electronics.

The front-end electronic circuitry, mounted on a daughter printed circuit board, is connected to a motherboard that has all of the necessary interface electronics to communicate with EPICS via a controller module and within the same electronics crate. A software state machine sequence was written within EPICS to control and operate WS/HS instrumentation (5). The state machine instructs the VI to move the wire and scraper to a specific location, acquire synchronous distribution data from either the wire or scraper, and triggers the IDL routine to normalise the acquired charge with a nearby toroidal current measurement, graph the normalised data, and write the distribution to a file. The sequence also instructs IDL to calculate the first through fourth moments, fit a gaussian distribution to the wire scanner data, and calculate the point at which the beam distribution disappears into the distribution background noise.

To plot the complete beam distribution for each axis, the wire scanner and two scraper data sets must be joined. To accomplish this joining, several analysis tasks are performed on the wire and scraper data including,

1) scraper data are spatially differentiated,
2) wire and scraper data are acquired with sufficient spatial overlap, and

The scraper data need only be normalised in the relative charge axis since the distances between each wire and scraper edge are known to within 0.25-mm. In addition, the first four moments and the point at which the beam distribution disappears into the noise are also calculated for the combined distribution data.

3 ACQUIRED DISTRIBUTIONS

Fig. 4 shows data from WS/HS #26 with some slight mismatch generated by increasing the field above nominal by 5% in the first matching quadrupole magnet. These typical WS/HS profiles show distributions with a dynamic range of > 10^5:1 and provide distribution information to > 5X to 7X times typical rms widths of the beam. The calculated rms widths are 1.10 and 1.13 mm for the horizontal and vertical distributions, respectively. The points at which the distributions rises out of the noise are 5.9 and –8.2 mm for the horizontal axis and 5.8 and –6.7 mm for the vertical axis.

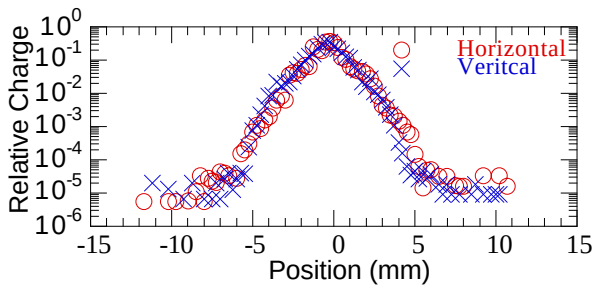

Figure 4. WS/HS distributions, such as #26 shown here, have a typical dynamic range of > 10^5:1.

4 WIRE AND SCRAPER PHYSICS

The choice of bias potential was determined by measuring the wire and scraper currents as a function of bias potential. The resulting data, displayed in fig. 5, show that the wire is optimally biased at -6 to -12 V and the scraper is optimally biased at +20 to +30 V.

The net wire current near the 0 V potential is approximately 15% higher than at either +6 V or –10 V. One proposed cause of the elevated net wire current is the interception of electrons and ions from off-energy protons ionising residual background gas - both of these ionised species creating further secondary emission. As the wire is biased negatively, the intercepted electrons are rejected causing a reduction in secondary emission, and as the wire is biased positively, the intercepted ions are rejected causing a reduction in secondary emission. If the intercepted electron-ion pairs are the mechanism for the elevated net current, the wire should be biased to not include this additional 15% net current component. Also note that as the wire bias is positively increased from 0 V to > +100 V, the wire secondary electron emission is inhibited and the net wire current reduces to very near collects positive ions with < -25 V bias potentials well after the beam pulse. This ion collection additionally limits the amount of negative bias that is applied to the wire for proper secondary emission operation.

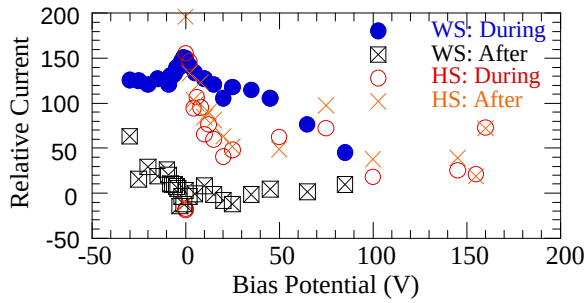

Figure 5. The above graph displays the wire scanner and halo scraper net current during and after the macropulse as a function of applied bias potential.

The scraper detection goal is to inhibit secondary emission and detect only 6.7-MeV protons. With 0 V applied to the scraper, the scraper net current is elevated by a factor of X3, likely from secondary emission. With approximately +25 V bias applied to the scraper, the secondary emission is almost entirely inhibited and the net current reduces to the nominal proton current. Also, note that with this +25 V bias, the data show that no ions appear to be collected after beam pulse.

5 SUMMARY

A wire scanner and halo scraper have been integrated into a beam profile instrument capable of 10^5:1 dynamic range. The scanner and scraper V-I curves show that the wire and scraper are optimally biased at –12 V and +25 V, respectively. We are presently acquiring halo data with these instruments and comparing these data to simulation halo models.

REFERENCES

[1] P. L. Colestock, et al., “The Beam Halo Experiment at the LEDA Facility: a First Test of the Core-Halo Model,” LINAC2000 Proceedings, SLAC-R-561, pp. 806-809.

[2] J. D. Gilpatrick, et al., "Beam Diagnostics Instrumentation for a 6.7-MeV Proton Beam Halo Experiment”, LINAC2000 Proceedings, SLAC-R-561, pp. 184-186.

[3] T. Wangler, et al., “Beam Halo in Proton Linac Beams,” LINAC2000 Proceedings, SLAC-R-561, pp. 341-345.

[4] R. Valdiviez, et al., “Intense Proton Core And Halo Beam Profile Measurement: Beam Line Component Mechanical Design”, LINAC2000 Proceedings, SLAC-R-561, pp. 181-183.

[5] L. Day, et al., “Control System for the LEDA 6.7-MeV Proton Beam Halo Experiment”, LINAC2000